University of
**Strathclyde**
Glasgow

# Strathprints Institutional Repository

http://strathprints.strath.ac.uk/

# SYSTEMS DESIGN OF A HYBRID SAIL POLE-SITTER

Matteo Ceriotti, Colin R. McInnes
*Advanced Space Concepts Laboratory, Department of Mechanical Engineering*
*University of Strathclyde, Glasgow G1 1XJ, United Kingdom*
*matteo.ceriotti@strath.ac.uk, colin.mcinnes@strath.ac.uk*

## ABSTRACT

This paper presents the preliminary systems design of a pole-sitter. This is a spacecraft that hovers over an Earth pole, creating a platform for full hemispheric observation of the polar regions, as well as direct-link telecommunications. To provide the necessary thrust, a hybrid propulsion system combines a solar sail with a more mature solar electric propulsion (SEP) thruster. Previous work by the authors showed that the combination of the two allows lower propellant mass fractions, at the cost of increased system complexity. This paper compares the pure SEP spacecraft with the hybrid spacecraft in terms of the launch mass necessary to deliver a certain payload for a given mission duration. A mass budget is proposed, and the conditions investigated under which the hybrid sail saves on the initial spacecraft initial mass. It is found that the hybrid spacecraft with near- to mid-term sail technology has a lower initial mass than the SEP case if the mission duration is 7 years or more, with greater benefits for longer duration missions. The hybrid spacecraft with far-term sail technology outperforms the pure SEP case even for short missions.

## INTRODUCTION

Solar electric propulsion (SEP) is a mature technology that provides a spacecraft with a relatively low thrust (of the order of a fraction of a Newton (Wallace, 2004)). Despite its high specific impulse, the thrust duration is always limited by the amount of propellant on-board.

In contrast, solar sailing (McInnes, 1999b) is a propellant-less spacecraft propulsion system: it exploits the solar radiation pressure due to solar photons impinging on a large, highly reflecting surface (the sail) to generate thrust. Despite the original idea of solar sailing is dating back to 1924 (Tsander, 1969), only recently has a spacecraft successfully deployed a solar sail for the first time (Yamaguchi et al. , 2010). Studies are ongoing (Baoyin and McInnes, 2006, Mengali and Quarta, 2009), including mission design (Kawaguchi et al. , 2009), due to the interesting potential of enabling missions that are not constrained by propellant mass availability. Solar sails appear to be suitable for potentially long duration missions that need a small, but continuous, amount of thrust. One example of such applications are interplanetary transfers (Mengali and Quarta, 2005), but solar sails have also been investigated to generate artificial equilibrium points, for example in the proximity of the Lagrange points of the Sun-Earth (Baoyin and McInnes, 2005) or Sun-Moon (Simo and McInnes, 2009b) system: the effect of the sail is that of creating regions in which the spacecraft can be stationary with respect to the two main bodies (McInnes, 1999a). These regions can be consistently far from the classical Lagrange points, thus enabling a whole range of new applications, from telecommunications and data relay to Earth and Moon observation.

Considering advantages and limitations of both SEP and solar sailing, the idea of a hybrid propulsion spacecraft, combining a solar sail and SEP arises. At the cost of increased spacecraft complexity, the two propulsion systems complement each other, cancelling their reciprocal disadvantages and limitations. In principle, SEP can provide thrust in any direction (through attitude maneuvers or a gimbal-mounted thruster), thus it can provide the missing acceleration component towards the Sun, that the sail cannot generate. Similarly, the hybrid spacecraft can be seen as an SEP spacecraft, in which an auxiliary solar sail provides part of the acceleration, enabling saving of propellant, and lower demand on the electric thruster, possibly with some intervals in which it could be turned off. In this sense, the hybrid spacecraft can be seen as a way to gradually introduce solar sails for space applications, and hence to reduce the advancement degree of difficulty $(AD^2)$ (Macdonald and McInnes, 2010) in the technology readiness level scale.

Hybridizing the two propulsion systems is a recent idea (Leipold and Götz, 2002), nevertheless research is flourishing in this almost completely unexplored field, investigating its potential for novel, interesting applications. Baig and McInnes (2008); proposed the use of a hybrid sail for generating artificial equilibria above $L_1$ in the Sun-Earth system for Earth observation; Mengali and Quarta (Mengali and Quarta, 2007a, b) investigated optimal interplanetary transfers to Venus and Mars using an indirect optimization method; Quarta et al. (2010) also considered hybridizing high thrust and an electric sail; Simo and McInnes exploited hybrid propulsion to find displaced periodic orbits in the Earth-Moon system (Simo and McInnes, 2009a); finally, JAXA has developed a hybrid solar sail demonstrator, IKAROS (Mori et al. , 2009).

In this work, hybrid propulsion is exploited to enable a mission in which the spacecraft is constantly above one of the Earth's poles, i.e. lying on the Earth's polar axis (Driver, 1980). This type of mission is known as pole-sitter. The pole-sitter provides a platform for continuous, real-time, medium-resolution observation of the Earth poles, with a full hemispheric view, as well as direct-link telecommunication and visibility of one of the Earth poles. It is well known that line-of-sight telecommunications to conventional spacecraft in geostationary orbits is not possible at high latitudes and polar regions, and telecommunication with polar regions will be a key issue in the future as changes to the arctic ice pack opens navigation channels for shipping. Also, the pole-sitter would offer real-time observation of the poles for climate science at modest resolution, in contrast to the periodic images that can be obtained by classical high-inclination orbits.

This mission concept has already been proposed in the literature. A stationary spacecraft in the rotating Sun-Earth system for Earth observation and data relay was investigated using a pure solar sail by McInnes and Mulligan (2003). This work was successively extended by Baig and McInnes (2008): in that paper, it was proposed to place a spacecraft in the same artificial equilibrium points of the Sun-Earth rotating system, but using hybrid SEP/sail propulsion. Finally, the orbital dynamics of a hybrid propulsion continuous pole-sitter was presented in a work by Ceriotti and McInnes (2010a), enabling a practical realization of the solar sail pole-sitter orbits proposed earlier by Forward (Forward, 1991). Ceriotti and McInnes (2010a) designed optimal orbits that follow the polar axis of the Earth in the restricted three-body problem. It was also shown that the hybrid propulsion spacecraft enabled consistent savings in propellant mass fraction. However, the hybrid propulsion spacecraft is inevitably more complex with respect to pure SEP: for example, the sail needs to be pointed to the right attitude to provide the correct force, as does the SEP thruster: this requires a gimbal system, that is unnecessary in the pure SEP spacecraft, as the whole spacecraft can be tilted using standard attitude control maneuvers. In this paper, the objective is to study the preliminary system design of a pole-sitter spacecraft, both in the SEP and hybrid propulsion cases, necessary to carry a given payload. The work will assess in which cases the hybrid spacecraft enables a lower initial wet mass with respect

to the SEP, for the same payload mass. The starting point for the mission design are the optimal orbits that were designed by Ceriotti and McInnes (2010a), to which we refer the reader for a complete description of the method and the results. In this paper, we will just present a brief overview of the equations of motion (section 1) and the optimization procedure (section 2). In section 3, the mass breakdown for the spacecraft will be explained in detail, followed by a comparison between the SEP case and the hybrid case, for a range of different technological parameters and mission durations.

## 1.  EQUATIONS OF MOTION

The circular restricted three-body problem (CR3BP) framework is considered (Sun-Earth-spacecraft). As is common, a synodic reference frame is used (Fig. 1). The mass of the Sun and the Earth are denoted $m_1$ and $m_2$ respectively, and $\boldsymbol{\omega} = \omega \hat{\mathbf{z}}$ the angular velocity of the system. The equations that describe the motion of the spacecraft of mass $m$ in this system are:

$$\ddot{\mathbf{r}} + 2\boldsymbol{\omega} \times \dot{\mathbf{r}} + \boldsymbol{\omega} \times (\boldsymbol{\omega} \times \mathbf{r}) - \nabla \left( \frac{1-\mu}{r_1} + \frac{\mu}{r_2} \right) = \mathbf{a}_s + \mathbf{a}_T \tag{1}$$

where $\mathbf{r}$ is the position vector, $\mathbf{a}_s$ is the acceleration due to the solar radiation pressure on the spacecraft sail, $\mathbf{a}_T = \mathbf{T}/m$ is the acceleration from the solar electric propulsion (SEP) system, provided by thrust vector $\mathbf{T}$.

Equation (1) will be used in its canonical non-dimensional form, which assumes $\omega = 1$, $\mu = m_2/(m_1 + m_2)$, and the unit of distance is the separation of the two primaries. With these assumptions, the position along the $\hat{\mathbf{x}}$-axis of $m_1$ is $-\mu$, and the position of $m_2$ is $1 - \mu$. For the Earth-Sun system, $\mu = 3.0404 \cdot 10^{-6}$. The two vectors $\mathbf{r}_1$ and $\mathbf{r}_2$ represent the position of the spacecraft with respect to the Sun and the Earth, respectively (see Fig. 1).
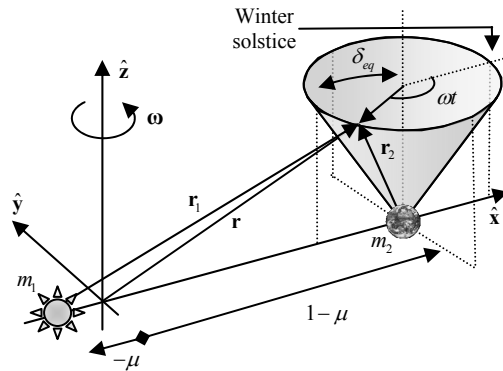


**Fig. 1. Restricted three-body problem and pole-sitter reference.**

The acceleration provided by a partially reflective, partially absorbing solar sail of total area $A$ can be expressed as (McInnes, 1999b):

$$\mathbf{a}_s = \frac{1}{2} \beta_0 \frac{m_0}{m} \frac{1-\mu}{r_1^2} \left[ g \cos \alpha \hat{\mathbf{n}} + h \sin \alpha \hat{\mathbf{t}} \right] \cos \alpha = \frac{1}{2} \beta_0 \frac{m_0}{m} \frac{1-\mu}{r_1^2} \sqrt{g^2 \cos^2 \alpha + h^2 \sin^2 \alpha} \cos \alpha \hat{\mathbf{m}} \tag{2}$$

Here $\hat{\mathbf{n}}$ is the component normal to the sail and $\hat{\mathbf{t}}$ parallel to it, in the plane of the Sun vector (Fig. 2a). $\beta_0$ is the *system lightness number* (ratio of solar pressure acceleration to gravitational acceleration) at the beginning of the mission, $\beta_0 = \sigma^* A / m_0$ : values of $\beta_0$, ranging from 0 (pure SEP) to 0.05 can be assumed for near- to mid-term technology (Dachwald et al. , 2006). In addition, $m_0$ and $m$ are the spacecraft mass at the beginning of the mission and at any given time, respectively. Note that, in the hybrid case, the spacecraft mass varies in general, due to the SEP propellant consumption, and so does the acceleration from the sail. The parameter $\sigma^* \cong 1.53 \cdot 10^{-3}$ kg$/m^2$ is the critical sail loading.

The sail acceleration is controlled by its attitude: the vector $\hat{\mathbf{n}}$ can be described using the so-called *cone angle* $\alpha$ (angle between $\hat{\mathbf{n}}$ and $\hat{\mathbf{r}}_1$, see Fig. 2a) and the *clock angle* $\delta$ (angle measured around $\hat{\mathbf{r}}_1$, starting from the vertical plane, of the component of $\hat{\mathbf{n}}$ perpendicular to $\hat{\mathbf{r}}_1$, see Fig. 2b). In the hybrid spacecraft, thin film solar cells (TFSC) cover an area $A_{TF} = 0.05A$ on the sail, and are used to power the SEP thruster. The area ratio is a conservative estimation based on previous studies (Baig and McInnes, 2008) and the IKAROS mission (Kawaguchi, Mimasu, 2009), and it is used to compute the optimal orbits. The actual value of this area depends on the spacecraft technology parameters, as well as the selected orbit, and it will be computed in section 3.

The direction of the acceleration $\hat{\mathbf{m}}$ is related to $\hat{\mathbf{n}}$ through the coefficients $g$ and $h$ (Baig and McInnes, 2008), which can be computed as a function of the reflectivity of the sail, $\tilde{r}_s = 0.9$, and of the thin film, $\tilde{r}_{TF} = 0.4$ (Leipold and Götz, 2002):

$$g = 1 + \tilde{r}_s + \frac{A_{TF}}{A}\left(\tilde{r}_{TF} - \tilde{r}_s\right); \qquad h = 1 - \tilde{r}_s - \frac{A_{TF}}{A}\left(\tilde{r}_{TF} - \tilde{r}_s\right) \tag{3}$$

The thrust of the SEP is assumed to be variable and mounted on a gimbal, and thus steerable. This adds three more controls to the spacecraft: thrust direction and magnitude. The propellant mass flow $\dot{m}$ is related to the thrust through Newton's law and the conservation of mass:

$$\dot{m} = T / I_{sp} g_0 \tag{4}$$

where we consider a specific impulse $I_{sp} = 3200$ s (based on current ion engine technology (existing NSTAR/DS1 (Brophy, 2003)) and $g_0 = 9.81$ m$/s^2$ .
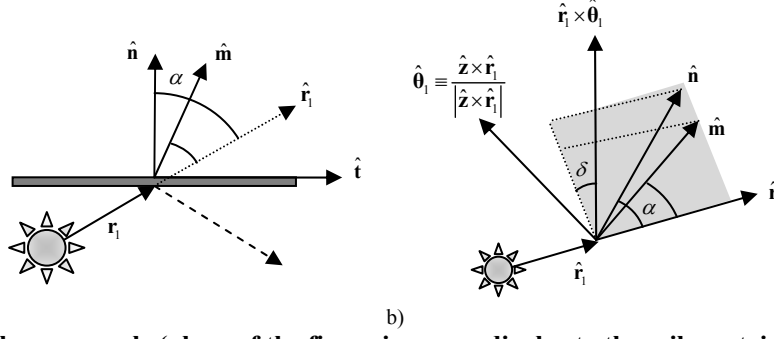
Fig. 2. a) Definition of the cone angle (plane of the figure is perpendicular to the sail, containing the Sun vector $r_1$). b) Solar sail cone and clock angles.

## 2. POLE-SITTER ORBITS

A pole-sitter spacecraft is constantly aligned with the polar axis of the Earth. We can consider that the polar axis of the Earth does not change its direction while the Earth is orbiting the Sun. In the synodic reference frame, the same axis rotates with a motion of apparent precession: its angular velocity is $-\boldsymbol{\omega}$ (refer to Fig. 1). Therefore, the polar axis spans a full conical surface every year. The cone half angle is the tilt of the axis relative to the ecliptic, i.e. $\delta_{eq} = 23.5 \text{ deg}$. The position of the spacecraft is to be constrained to follow the apparent precession of the polar axis, and hence maintain the pole-sitter condition. It is assumed that the spacecraft is injected at time $t_0 = 0$ at the winter solstice, and therefore the pole-sitter is on the cone at position:

$$
\mathbf{r}(t) = \begin{bmatrix} d(t)\sin\delta_{eq}\cos\omega t + (1-\mu) \\ -d(t)\sin\delta_{eq}\sin\omega t \\ d(t)\cos\delta_{eq} \end{bmatrix} \tag{5}
$$

where $d(t)$ is the distance from the center of the Earth and is a continuous function of time. The North Pole case is considered.

In this work, we use optimal periodic pole-sitter orbits that minimize the SEP propellant consumption over a period (one year), while maintaining the pole-sitter condition (5) at each instant during the mission. Optimal orbits are defined in terms of evolution over one year of the states (position, velocity, mass), and controls (sail cone and clock angles, SEP thrust direction and magnitude). The optimization process is performed in two steps: the first, which aims at finding a first guess solution, and the second, which locally optimizes the first guess. Details of the optimization process are covered in (Ceriotti and McInnes, 2010a). Here we provide a brief outline of the procedure for sake of completeness. The first guess is generated by using a shape-based approach, in which a specific orbit for the spacecraft and initial mass $m_0$ are assigned. Then, the controls that enable that orbit are obtained from the equations of motion with an iterative process. The orbit is discretized into a finite number of points in time. At each point, the sail cone and clock angles are computed numerically, minimizing the magnitude of the SEP acceleration. Once $\mathbf{a}_s$ is known, $\mathbf{a}_T$ can be computed by differencing. Assuming that the thrust remains constant from one point to the next along the orbit, Eq. (4) can be integrated to find the mass change. With this new value of mass, the procedure iterates on the next point on the orbit. The subsequent optimal control problem finds the orbit $\mathbf{r}(t)$ and the control

history that minimizes the propellant consumption of the spacecraft after one orbital period, subject to the boundary condition of periodicity and the pole-sitter constraint (5). A direct method based on pseudo-spectral transcription is used: the tool, named PSOPT, was created and coded in C++ and is freely available to use (Becerra, 2010). Note that the solutions found through the shape-based approach do not, in general, minimize propellant consumption. However, it was verified that, if the shape based approach is used on an orbit that is the result of an optimization, the control history, and thus also the propellant mass, is very similar to the optimal one.

Fig. 3, from Ceriotti and McInnes (2010a), shows an example of a particular pole-sitter orbit, in which the distance of the spacecraft from the Earth is constant. It also shows the acceleration vector fields (sail, SEP and total) and sail normal. Since the path of this orbit can be described analytically, the shape-based method can find the optimal control. Instead, Fig. 4 shows a family of optimal orbits, found by solving the optimal control problem. Here the spacecraft can vary its altitude, however in this specific case a constraint on the maximum distance from the Earth was enforced.
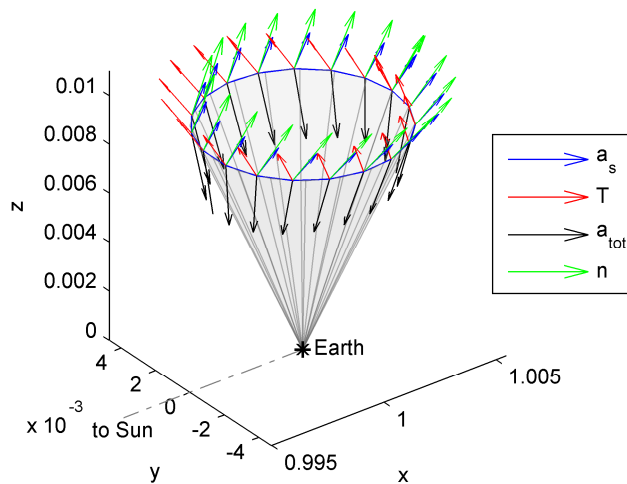


**Fig. 3. Acceleration vectors and sail normal along a constant-distance pole-sitter orbit.**
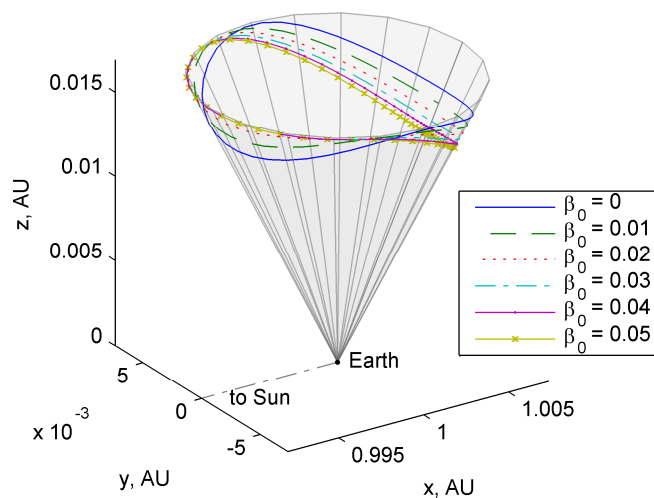


**Fig. 4. Optimal orbits, constrained to less than 0.01831 AU from the Earth, for different values of $\beta_0$.**

## 3. SYSTEM DESIGN

By comparing optimal solutions for pure SEP and hybrid spacecraft, it is found that the latter requires a lower propellant mass fraction. However, it is a more complex system, mainly due to the presence of the solar sail and the need to have a gimbaled thruster. Due to the additional subsystem mass, we need to assess the conditions at which the hybrid system allows a greater payload mass $m_{pl}$, with the same initial spacecraft mass $m_0$, or vice-versa a smaller launch mass for the same payload.

For the sake of comparison, the technological assumptions and mass split are based on (Baig and McInnes, 2008). In that work, the authors computed the requirements for a spacecraft to be stationary in the Sun-Earth rotation frame, placed at 0.01831 AU above the North Pole at the summer solstice (hence above the Lagrange point $L_1$). Here the distance is constrained to be less than or equal to this value, for consistency, leading to optimal orbits such as those in Fig. 4.

### 3.1 Mass Breakdown Model

For a preliminary mass budget, the total spacecraft mass can be split as:

$$m_0 = m_{prop} + m_{tank} + n_{thrusters}\left(m_{SEP} + m_{gimbal}\right) + m_s + m_{TF} + m_{rad} + m_{pl} \tag{6}$$

The definition of the symbols are described in the following. $m_{prop}$ is the propellant mass necessary for a given mission of duration $t_{mission}$. The mass of the tanks $m_{tank}$ is a function of the propellant mass (Gershman and Seybold, 1999):

$$m_{tank} = 0.1 m_{prop} \tag{7}$$

Two thrusters were considered ($n_{thrusters} = 2$) for redundancy, and to prevent excessive degradation during the mission. Note that this introduces the necessity of a gimbal system to prevent the misalignment of the thrust vector provided by both thrusters with respect to the center of mass of the spacecraft. The mass of the engine $m_{SEP}$ is function of its power, through

$$m_{SEP} = k_{SEP} P_{SEP,max} \tag{8}$$

with $k_{SEP} = 20\,\text{kg/kW}$ (Brophy, 2003). The maximum power $P_{SEP,max}$ required by the SEP subsystem is computed as a function of the maximum thrust $T_{max}$ required during the mission, as

$$P_{SEP,max} = T_{max} I_{sp} g_0 / 2\eta_{SEP} \tag{9}$$

where $\eta_{SEP} = 0.7$ is the efficiency of converting electrical energy (Kitamura et al. , 2007).

Then, $m_{gimbal}$ is the SEP thruster gimbal mass, and it is assumed to be proportional to the thruster mass:

$$m_{gimbal} = \rho_{gimbal} m_{SEP} \tag{10}$$

As noted before, for the pure SEP spacecraft the gimbal is responsible for compensating the thrust misalignment due to the presence of two engines. However, the attitude of a three-axis stabilized spacecraft can be changed to orientate the thrust vector in the required direction. Instead, in the hybrid case, the sail is fixed to the spacecraft bus, whose attitude is determined by the sail. Therefore, a more sophisticated gimbal system is required to point the thrust vector independently from the

spacecraft (within limits due to the system configuration). It was decided to select $\rho_{gimbal} = 0.3$ for the hybrid case (Gershman and Seybold, 1999); instead $\rho_{gimbal} = 0.1$ for the pure SEP.

The total sail area (highly reflective surface + TFSC) can be computed starting from the assumed values of $\beta_0$ and $m_0$. The mass of the thin film is proportional to its area:

$$m_{TF} = \sigma_{TF} A_{TF} \tag{11}$$

where $\sigma_{TF} = 100$ g/m$^2$ (Leipold and Götz, 2002). The area of the thin film can be estimated as a function of the maximum power. For the pure SEP spacecraft, the solar panels are usually kept perpendicular to the Sun vector, and therefore the area of TFSC necessary to guarantee the required power is

$$A_{TF} = P_{SEP,max}/W\eta_{TF} \tag{12}$$

with $\eta_{TF} = 0.05$ due to the relatively low efficiency of the thin film, and energy flux density of the Sun $W = 1367$ W/m$^2$ at 1 AU. In the hybrid spacecraft, instead, the TFSC is part of the reflective surface, and therefore its pitch with respect to the Sun vector is given by the clock angle of the sail $\alpha = \alpha_{T_{max}}$ at the instant when the maximum thrust is required. Consequently, in the hybrid case, the area of the TFSC shall be augmented according to

$$A_{TF} = P_{SEP,max}/W\eta_{TF} \cos\alpha_{T_{max}} \tag{13}$$

The area of the sail is simply $A_s = A - A_{TF}$, and its mass is $m_s = \sigma_s A_s$, where $\sigma_s$ is the mass per unit area of the sail, or *sail loading*, which is a critical parameter that depends on the solar sail technology. It is expected that near-term technological developments should allow values of 10 g/m$^2$ (Dachwald, 2004). Ultra-thin (around 2 µm of thickness) sails are expected in the mid- to far-term timeframe (Murphy et al. , 2002) and can lead, for large sails, to loadings on the order of 5 g/m$^2$.

The TFSC are sized on the maximum power needed, assuming that they can be perpendicular to the Sun in the pure SEP spacecraft, and at the sail attitude for the hybrid spacecraft. However, the thrust, and hence the power required during the whole mission is variable. It was found that for some configurations, the SEP thrust is not needed for long periods of time during the orbit (around summer). In these cases, while the solar panels of the SEP spacecraft can be tilted, such that they generate only the power needed at every instant of time, this is not possible on the hybrid spacecraft. The attitude of the TFSC is once again constrained to that of the sail, and therefore they will keep producing power. Radiators can be employed to dissipate the excess power. Radiators are sized considering the minimum SEP thrust throughout the mission, and calculating the excess of power $P_{d,max}$ generated by the panels at that instant of time, and so the power that is to be dissipated. It is then assumed:

$$m_{rad} = 0.0086 \text{ kg/W} \cdot P_{d,max} \tag{14}$$

where the coefficient is found using a specific power of 350 W/ m$^2$ (value achievable in deep space (Wertz and Larson, 1999), p. 440), and a specific weight of 3 kg/m$^2$, considering that the radiators can be mounted on the back side of the TFSC, sharing the structure. For the pure SEP, $m_{rad} = 0$ for the reasons stated above.

Eq. (6) allows us to implicitly find $m_0$ for a given payload mass $m_{pl}$. Given a guess value for the initial mass $m_0 = m_{0,guess}$, first the optimal 1-year periodic orbit is determined solving the optimal control problem. This orbit is then used to compute $m_{prop}$ for the entire mission duration, using the inverse method. An iterative Newton-Raphson method is used to solve Eq. (6): at every iteration the propellant mass and the mass of all the other subsystems are re-computed, leading to a new value of $m_0$, until convergence.

## 3.2    Results

In this section we propose a comparison in terms of launch mass and deliverable payload mass between the pure SEP spacecraft and the hybrid spacecraft.

Fig. 5 shows the initial mass (logarithmic scale) of the spacecraft needed for $m_{pl} = 100$ kg, as a function of the lightness number $\beta_0$, and for three values of $\sigma_s$: 10 g/m², 7.5 g/m² and 5 g/m². The pure SEP case is also represented, when feasible, as a marker along $\beta_0 = 0$. For comparison with the hybrid cases, dashed horizontal lines were added. Different colors and markers refer to different mission durations, from 5 to 10 years. Also, the mass values of the pure SEP spacecraft do not obviously depend on the sail loading, and hence they are the same in the three plots.

The first thing to note is the discontinuity in the initial mass at $\beta_0 = 0$: the mass of the sail grows proportionally to its size (and so to $\beta_0$); however, adding a small sail implies also adding radiators and a heavier gimbal system. The masses of these two are not proportional to the sail size, and this explains why for small values of $\beta_0$ the pure SEP option is always more convenient.

It is also interesting to note that not all the mission durations are achievable with a given $\beta_0$: for example, the solution with pure SEP does not exist for missions of 9 years and longer. In the same way, if the sail loading is 7.5 g/m², then 8 year solutions only exist for solutions with $\beta_0 < 0.04$. In the same way, for $\sigma_s = 5$ g/m², the 9 year mission only exist for $\beta_0 > 0.02$, and the 10-year mission is only possible for $0.03 < \beta_0 < 0.04$, albeit with very high initial mass. Fig. 6 displays a magnification of Fig. 5c for the lower values of $m_0$.
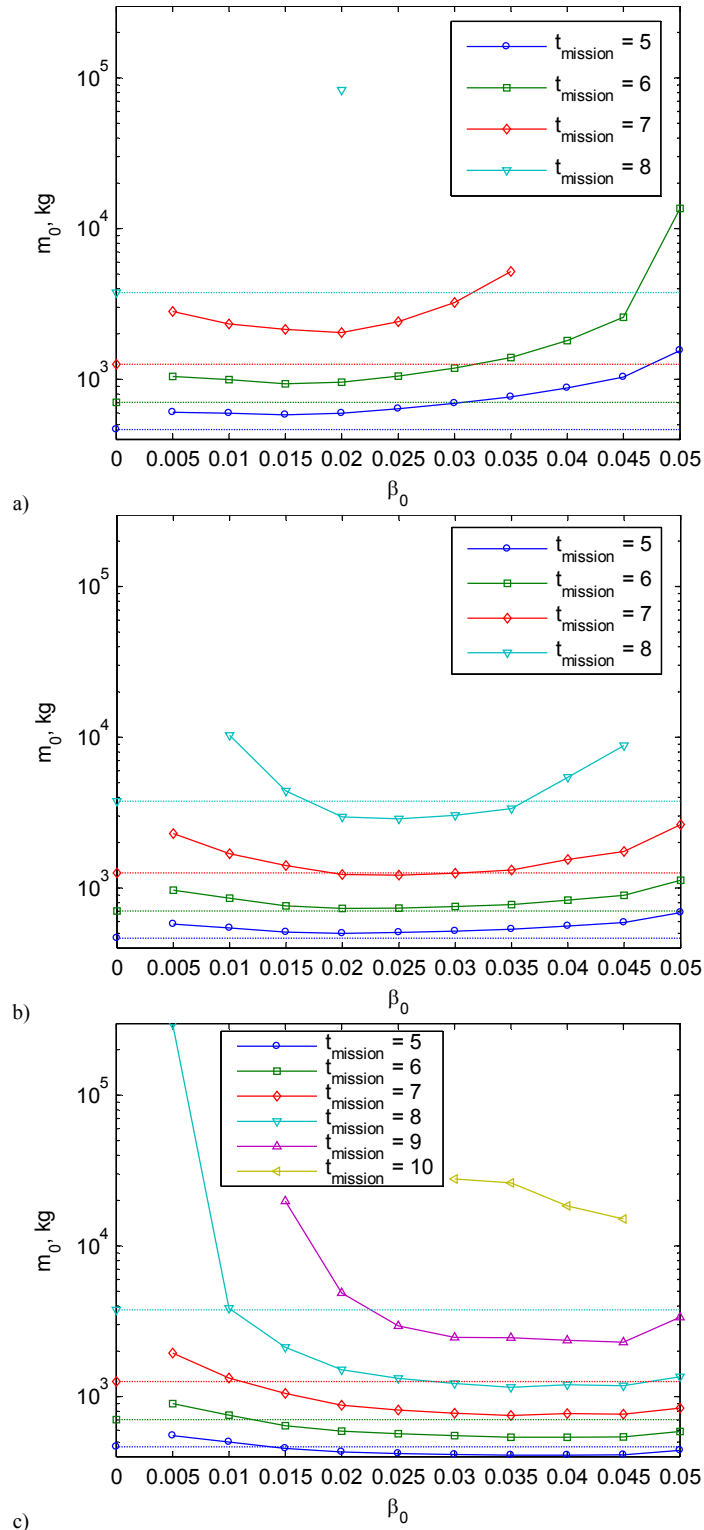
**Fig. 5. Initial mass (logarithmic scale) required for a 100 kg payload, for pure SEP and hybrid spacecraft as a function of $\beta_0$, for three different values of sail loading: a) $\sigma_s = 10$ g/m$^2$; b) $\sigma_s = 7.5$ g/m$^2$; c) $\sigma_s = 5$ g/m$^2$. Pure SEP value extended (dashed line) for comparison with hybrid.**
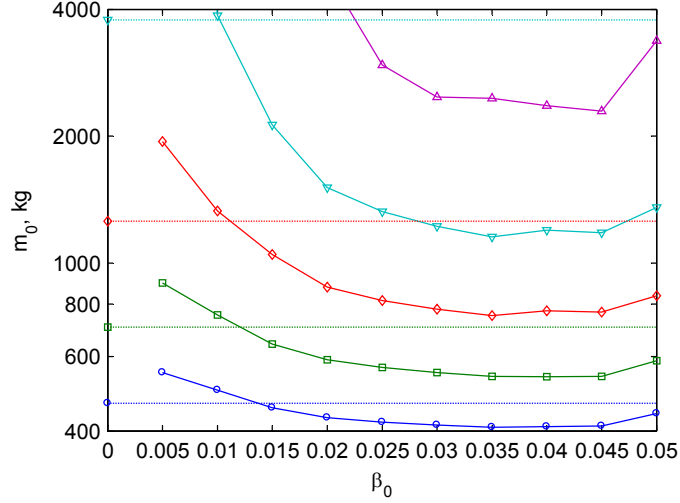
**Fig. 6. Magnification of the bottom part of Fig. 5c.**

Also, Fig. 5 shows that for $\sigma_s = 10 \text{ g/m}^2$ (and therefore also for higher values) the hybrid spacecraft is never advantageous over the pure SEP case. Finally, depending on $\sigma_s$ and the mission duration, the optimal design point for minimizing the initial mass of the hybrid spacecraft is different in terms of $\beta_0$: for example, for $\sigma_s = 5 \text{ g/m}^2$ and up to 8 years, the lowest mass is found at about $\beta_0 = 0.035$, while $\beta_0 = 0.045$ enables the lowest mass for 9 and 10 years. but this value decreases to $\beta_0 = 0.025$ for the other two values of sail loading that were considered. If $\sigma_s = 7.5 \text{ g/m}^2$, the minima are found for $\beta_0 \in [0.02, 0.025]$, depending on the mission duration, and for $\sigma_s = 10 \text{ g/m}^2$ they are found in $\beta_0 \in [0.015, 0.02]$.

We propose here different mission scenarios, which differ in their nominal duration: 5, 8 and 10 years respectively. For each one of these, we compare the pure SEP case with the hybrid one. The design points are described in Table 1: only values of sail loading that enable mass saving with respect to the SEP are shown. The same table also shows the mass breakdown for the different spacecraft, as well as the size of the sail required. For each case, the system lightness number that minimizes the spacecraft mass is selected from the curves in Fig. 5. For the 5-year mission, hybrid propulsion enables a small mass saving only if the sail loading is 5 g/m² (or less). However, the improvement of the hybrid spacecraft with respect to the pure SEP spacecraft becomes important considering the longer 8-year mission: for this mission, sail loadings below 7.5 g/m² offer consistent advantages. For pure SEP, a 3773 kg spacecraft and a maximum thrust of 660 mN is required. Instead, adding a mid-term sail brings these values down to 2871 kg and 435 mN. As expected, further improvements are obtained for the far-term spacecraft: 1153 kg and 167 mN. For the 10-year mission, the spacecraft mass and sail size are huge, and even if this mission is feasible only considering hybrid propulsion, it is not of any practical realization in the near future. Note also that this work does not consider any degradation of the solar sail, which would affect the performance especially in longer missions. This is subject of another study (Ceriotti and McInnes, 2010b), in which a control system is designed to compensate this effect.

**Table 1. Mass split for different design points, varying lightness number, mission duration and sail loading, for $m_{pl}$ = 100 kg.**

| | 5 | | 8 | | | 10 |
|---|---|---|---|---|---|---|
| $t_{mission}$ , y | | | | | | |
| $\sigma_s$ , g/m$^2$ | SEP | 5 | SEP | 7.5 | 5 | 5 |
| $\beta_0$ | | 0.035 | | 0.025 | 0.035 | 0.045 |
| $m_0$ , kg | 465 | 408 | 3773 | 2871 | 1153 | 15,080 |
| $m_{pl}$ , kg | 100 | 100 | 100 | 100 | 100 | 100 |
| $m_{rad}$ , kg | 0 | 6.98 | 0 | 54.3 | 19.3 | 292 |
| $m_{gimbal}$ , kg | 3.65 | 7.97 | 29.6 | 58.6 | 22.5 | 282 |
| $m_{SEP}$ , kg | 36.5 | 26.6 | 296 | 195 | 75.1 | 939 |
| $m_{prop}$ , kg | 257 | 165 | 2727 | 1670 | 635 | 9017 |
| $m_s$ , kg | - | 46.5 | - | 350 | 131 | 2212 |
| $m_{TF}$ , kg | 2.67 | 3.09 | 21.6 | 21.8 | 8.76 | 115 |
| $A_s$ , m$^2$ | - | 9305 | - | 46,692 | 26,296 | 442,382 |
| $A_{TF}$ , m$^2$ | 27 | 30.9 | 216 | 218 | 87.6 | 1151 |
| $P_{SEP,max}$ , W | 1824 | 1328 | 14,796 | 9762 | 3753 | 46,961 |
| $T_{max}$ , mN | 81.4 | 59.2 | 660 | 435 | 167 | 2094 |

The trade-off between payload mass, mission duration and initial mass is presented in Fig. 7 to Fig. 9. Each figure refers to a different type of spacecraft: Fig. 7 is for pure SEP; (c) and (d) to a near-term hybrid sail; finally, (e) and (f) to a far-term hybrid spacecraft. It can be seen that the system mass scales almost linearly with the payload mass (having fixed all the other parameters), while it scales approximately exponentially with the mission duration. This is reflected in the steep increase in the system mass for longer duration missions.
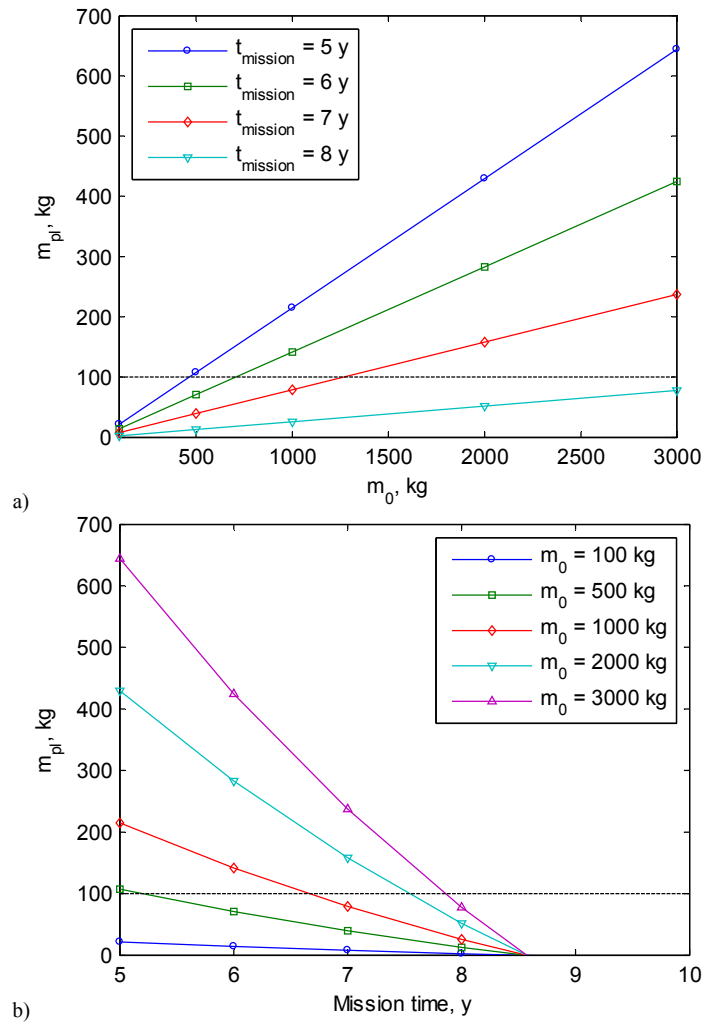
Fig. 7. Pure SEP spacecraft: payload mass as a function of initial mass (a) and mission duration (b).
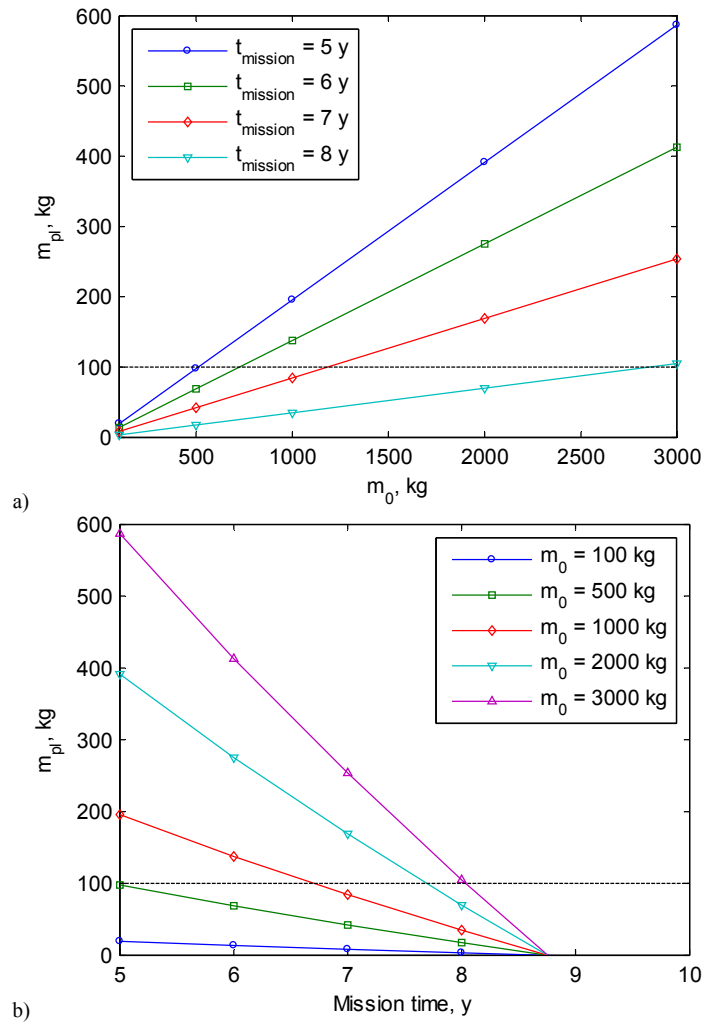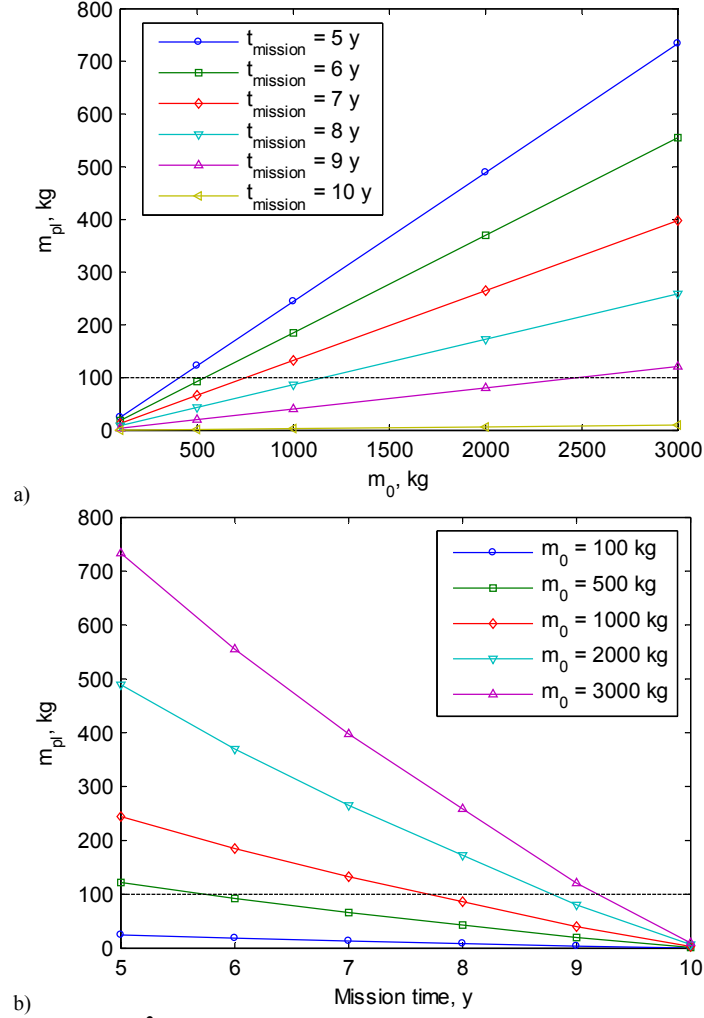
a)



b)

**Fig. 8. Hybrid spacecraft with $\sigma_s = 7.5$ g/m$^2$ and $\beta_0 = 0.025$: payload mass as a function of initial mass (a) and mission duration (b).**

**Fig. 9.** Hybrid spacecraft with $\sigma_s = 5$ g/m$^2$ and $\beta_0 = 0.035$: payload mass as a function of initial mass (a) and mission duration (b).

To explain the steep increase of $m_0$ with $t_{mission}$, and justify the trend of the graphs in Fig. 7, we consider a simple 1D case for illustration. Consider a rocket of initial wet mass $m_0$ to be accelerated with constant acceleration $a$. Note the key point here: usually a rocket provides a constant thrust, not acceleration. The differential equation for the rocket mass is:

$$\dot{m}(t) = -\frac{m(t)a}{I_{sp}g_0} \tag{15}$$

Now we can express the mass budget for the rocket:

$$m_0 = m_{pl} + m_{prop} + km_{prop} + hF_{max} \tag{16}$$

Here $m_{pl}$ is the payload mass, $m_{prop}$ is the propellant mass needed for a given mission duration $t_{mission}$ and the other two terms represent two inert masses: the first is a function of the propellant mass (e.g. the tank), the second is a function of the maximum thrust (e.g. the engine).

The propellant mass can be computed as:

$$m_{prop} = m_0 - m\left(t_{mission}\right) \tag{17}$$

Since $a$ is constant, the maximum thrust is certainly at the initial time, when the mass is highest. So:

$$F_{max} = m_0 a \tag{18}$$

We are interested in correlating the payload mass with the final time $t_{mission}$. The final mass can be found by integrating Eq. (15), noting once again that $a$ is constant, and obtaining:

$$m\left(t_{mission}\right) = m_0 e^{-\frac{a}{I_{sp} g_0} t_{mission}} \tag{19}$$

Substituting Eq. (19) and Eq. (18) into Eq. (16) we have:

$$m_{pl} = -\left(k + ha\right) m_0 + \left(1 + k\right) m_0 e^{-\frac{a}{I_{sp} g_0} t_{mission}} \tag{20}$$

Since the coefficient $-\left(k + ha\right)$ is strictly negative, the curve $m_{pl}\left(t_{mission}\right)$ intersects the $x$ axis at some point (in which $m_{pl} = 0$), that depends only on the engineering coefficients $k$, $h$ and the acceleration $a$, but not on the initial mass $m_0$. Therefore, an increase of propellant mass would increase the payload mass, but not the maximum mission duration. If instead $k = h = 0$ (no inert mass), then the final time $t_{mission}$ goes to infinity, but no payload can be carried ($m_{pl} \to 0$ for $t_{mission} \to +\infty$). An analogous behavior is noted in the pole-sitter spacecraft. Note that this result applies to other missions, in which the acceleration profile is assigned: this includes non-Keplerian orbits (NKO) and artificial equilibria, in which a constant acceleration is provided to counteract the natural dynamics of the system.

**CONCLUSIONS**

In this paper, we investigated the conditions for a hybrid pole-sitter to enable not only fuel saving, but a smaller initial spacecraft mass with respect to a pure SEP spacecraft, for a given payload mass. To this aim, we considered a mass budget model that included relevant subsystems. The additional system complexity of the hybrid spacecraft could therefore be modeled. It was found that, with near- to mid-term sail technology, the hybrid spacecraft has a lower initial mass than the SEP case if the mission duration is 7 years or more, with greater benefit for longer missions. Assuming far-term sail technology, then the hybrid spacecraft outperforms the pure SEP case even for short missions.

Moreover, it was found that the system mass scales linearly with the payload mass; however, the lifetime is limited by the type of propulsion system, no matter the initial mass: the pure SEP is infeasible for missions longer than 8 years, while the addition of a solar sail extends the mission duration. It is therefore proposed that a hybrid solar sail and SEP system may be a means of enabling challenging long-duration, high energy missions by using a modest solar sail to enhance the performance of existing SEP technology.

## ACKNOWLEDGMENTS

## REFERENCES

Baig, S., McInnes, C.R. Artificial three-body equilibria for hybrid low-thrust propulsion. J Guid Control Dynam, vol. 31, n. 6, pp. 1644-1655, 2008. doi: 10.2514/1.36125

Baoyin, H., McInnes, C.R. Solar sail orbits at artificial Sun-Earth libration points. J Guid Control Dynam, vol. 28, n. 6, pp. 1328-1331, 2005. doi: 10.2514/1.14598

Baoyin, H., McInnes, C.R. Solar sail equilibria in the elliptical restricted three-body problem. J Guid Control Dynam, vol. 29, n. 3, pp. 538-543, 2006. doi: 10.2514/1.15596

Becerra, V.M. Solving complex optimal control problems at no cost with PSOPT. *IEEE Multi-conference on Systems and Control*, IEEE, Yokohama, Japan, pp. 1391-1396, 2010.

Brophy, J. Advanced ion propulsion systems for affordable deep-space missions. Acta Astronautica, vol. 52, n. 2-6, pp. 309-316, 2003. doi: 10.1016/S0094-5765(02)00170-4

Ceriotti, M., McInnes, C.R. An Earth pole-sitter using hybrid propulsion. *AIAA/AAS Astrodynamics Specialist Conference*, AIAA-2010-7830, AIAA, Toronto, Ontario, Canada, 2010a.

Ceriotti, M., McInnes, C.R. Hybrid solar sail and SEP propulsion for novel Earth observation missions. *61st International Astronautical Congress (IAC 2010)*, IAC-10.C4.6.8, International Astronautical Federation, Prague, Czech Republic, 2010b.

Dachwald, B. Solar sail performance requirements for missions to the outer solar system and beyond. *55th International Astronautical Congress (IAC 2004)*, IAC-04-S.P.11, International Astronautical Federation, Vancouver, Canada, 2004.

Dachwald, B., Mengali, G., Quarta, A.A., Macdonald, M. Parametric model and optimal control of solar sails with optical degradation. J Guid Control Dynam, vol. 29, n. 5, pp. 1170-1178, 2006. doi: 10.2514/1.20313

Driver, J.M. Analysis of an arctic polesitter. Journal of Spacecraft and Rockets, vol. 17, n. 3, pp. 263-269, 1980. doi: 10.2514/3.57736

Forward, R.L. Statite: a spacecraft that does not orbit. Journal of Spacecraft and Rockets, vol. 28, n. 5, pp. 606-611, 1991. doi: 10.2514/3.26287

Gershman, R., Seybold, C. Propulsion trades for space science missions. Acta Astronautica, vol. 45, n. 4-9, pp. 541-548, 1999. doi: 10.1016/S0094-5765(99)00174-5

Kawaguchi, J.i., Mimasu, Y., Mori, O., Funase, R., Yamamoto, T., Tsuda, Y. IKAROS - Ready for lift-off as the world's first solar sail demonstration in interplanetary space. *60th International Astronautical Congress (IAC 2009)*, IAC-09-D1.1.3, International Astronautical Federation, Daejeon, Korea, 2009.

Kitamura, S., Ohkawa, Y., Hayakawa, Y., Yoshida, H., Miyazaki, K. Overview and research status of the JAXA 150-mN ion engine. Acta Astronautica, vol. 61, n. 1-6, pp. 360-366, 2007. doi: 10.1016/j.actaastro.2007.01.010

Leipold, M., Götz, M. Hybrid photonic/electric propulsion. Kayser-Threde GmbH, Report Technical Report SOL4-TR-KTH-0001, ESA contract No. 15334/01/NL/PA, Munich, Germany, 2002.

Macdonald, M., McInnes, C.R. Solar sail mission applications and future advancement. *2nd International Symposium on Solar Sailing (ISSS 2010)*, edited by Kezerashvili, R.Y., New York, NY, USA, pp. 7-26, 2010.

McInnes, C.R. Artificial Lagrange points for a partially reflecting flat solar sail. J Guid Control Dynam, vol. 22, n. 1, pp. 185-187, 1999a. doi: 10.2514/2.7627

McInnes, C.R. Solar sailing: technology, dynamics and mission applications. Springer-Verlag, Berlin, 1999b.

McInnes, C.R., Mulligan, P. Final report: telecommunications and Earth observations applications for polar stationary solar sails. National Oceanographic and Atmospheric Administration (NOAA)/University of Glasgow, Department of Aerospace Engineering, 2003. www.osd.noaa.gov/rpsi/polesitter.telecommunications.pdf [Retrieved 16 November 2010]

Mengali, G., Quarta, A.A. Optimal three-dimensional interplanetary rendezvous using nonideal solar sail. J Guid Control Dynam, vol. 28, n. 1, pp. 173-177, 2005. doi: 10.2514/1.8325

Mengali, G., Quarta, A.A. Tradeoff performance of hybrid low-thrust propulsion system. Journal of Spacecraft and Rockets, vol. 44, n. 6, pp. 1263-1270, 2007a. doi: 10.2514/1.30298

Mengali, G., Quarta, A.A. Trajectory design with hybrid low-thrust propulsion system. J Guid Control Dynam, vol. 30, n. 2, pp. 419-426, 2007b. doi: 10.2514/1.22433

Mengali, G., Quarta, A.A. Solar sail trajectories with piecewise-constant steering laws. Aerospace Science and Technology, vol. 13, n. 8, pp. 431-441, 2009. doi: 10.1016/j.ast.2009.06.007

Mori, O., Sawada, H., Funase, R., et al. Development of first solar power sail demonstrator - IKAROS. *21st International Symposium on Space Flight Dynamics (ISSFD 2009)*, CNES, Toulouse, France, 2009.

Murphy, D.M., Murphey, T.W., Gierow, P.A. Scalable solar-sail subsystem design considerations. *43rd AIAA/ASME/ASCE/AHS/ASC Structures, Structural Dynamics, and Materials Conference*, AIAA-2002-1703, American Institute of Aeronautics and Astronautics, Denver, Colorado, 2002.

Quarta, A.A., Mengali, G., Janhunen, P. Optimal interplanetary rendezvous combining electric sail and high thrust propulsion system. Acta Astronautica, vol. In Press, Corrected Proof, 2010. doi: 10.1016/j.actaastro.2010.01.024

Simo, J., McInnes, C.R. Displaced periodic orbits with low-thrust propulsion. *19th AAS/AIAA Space Flight Mechanics Meeting*, AAS 09-153, American Astronautical Society, Savannah, Georgia, USA, 2009a.

Simo, J., McInnes, C.R. Solar sail orbits at the Earth-Moon libration points. Communications in Nonlinear Science and Numerical Simulation, vol. 14, n. 12, pp. 4191-4196, 2009b. doi: 10.1016/j.cnsns.2009.03.032

Tsander, F.A. From a scientific heritage (Translation of "Iz nauchnogo naslediya"). NASA Technical Translation. NASA, Report NASA-TT-F-541, 1969.09/11/2010]

Wallace, N.C. Testing of the QinetiQ T6 thruster in support of the ESA BepiColombo Mercury mission. *Space Propulsion 2004 - 4th International Spacecraft Propulsion Conference, June 2, 2004 - June 4, 2004*, European Space Agency, Sardinia, Italy, pp. 479-484, 2004.

Wertz, J.R., Larson, W.J. Space mission analysis and design, third edition. Space technology library. Microcosm press/Kluwer Academic Publishers, El Segundo, California, USA, 1999.

Yamaguchi, T., Mimasu, Y., Tsuda, Y., Takeuchi, H., Yoshikawa, M. Estimation of solar radiation pressure force for solar sail navigation. *61st International Astronautical Congress (IAC 2010)*, IAC-10-C1.6.4, International Astronautical Federation, Prague, Czech Republic, 2010.